Journal of the American College of Cardiology
© 2012 by the American College of Cardiology Foundation
Published by Elsevier Inc.

Vol. 59, No. 2, 2012
ISSN 0735-1097/$36.00
doi:10.1016/j.jacc.2011.08.066

PET/MRI of Inflammation in Myocardial Infarction

Won Woo Lee, MD, PHD,*† Brett Marinelli, BA,* Anja M. van der Laan, MD,‡ Brena F. Sena, BS,* Rostic Gorbatov, BS,* Florian Leuschner, MD,* Partha Dutta, PHD,* Yoshiko Iwamoto, BS,* Takuya Ueno, MD, PHD,* Mark P. V. Begieneman, BS,§ Hans W. M. Niessen, MD, PHD,§ Jan J. Piek, MD, PHD,‡ Claudio Vinegoni, PHD,* Mikael J. Pittet, PHD,* Filip K. Swirski, PHD,* Ahmed Tawakol, MD,‖ Marcelo Di Carli, MD,¶ Ralph Weissleder, MD, PHD,* Matthias Nahrendorf, MD, PHD*

Boston, Massachusetts; Seoul, Korea; and Amsterdam, the Netherlands

Objectives The aim of this study was to explore post–myocardial infarction (MI) myocardial inflammation.

Background Innate immune cells are centrally involved in infarct healing and are emerging therapeutic targets in cardiovascular disease; however, clinical tools to assess their presence in tissue are scarce. Furthermore, it is currently not known if the nonischemic remote zone recruits monocytes.

Methods Acute inflammation was followed in mice with coronary ligation by 18-fluorodeoxyglucose (^{18}FDG) positron emission tomography/magnetic resonance imaging, fluorescence-activated cell sorting, polymerase chain reaction, and histology.

Results Gd-DTPA–enhanced infarcts showed high ^{18}FDG uptake on day 5 after MI. Cell depletion and isolation data confirmed that this largely reflected inflammation; CD11b^{+} cells had 4-fold higher ^{18}FDG uptake than the infarct tissue from which they were isolated ($p < 0.01$). Surprisingly, there was considerable monocyte recruitment in the remote myocardium (approximately 10^4/mg of myocardium, 5.6-fold increase; $p < 0.01$), a finding mirrored by macrophage infiltration in the remote myocardium of patients with acute MI. Temporal kinetics of cell recruitment were slower than in the infarct, with peak numbers on day 10 after ischemia. Quantitative polymerase chain reaction showed a robust increase of recruiting adhesion molecules and chemokines in the remote myocardium (e.g., 12-fold increase of monocyte chemoattractant protein-1), although levels were always lower than in the infarct. Finally, matrix metalloproteinase activity was significantly increased in noninfarcted myocardium, suggesting that monocyte recruitment to the remote zone may contribute to post-MI dilation.

Conclusions This study shed light on the innate inflammatory response in remote myocardium after MI. (J Am Coll Cardiol 2012;59:153–63) © 2012 by the American College of Cardiology Foundation

Myocardial infarction (MI) triggers a robust local inflammatory response (1,2). On the cellular level, the innate immune system reacts to ischemic injury with mobilization of neutrophils and monocytes during the first weeks after ischemia. The amplitude and duration of inflammation and its timely resolution influence post-MI remodeling and the evolution of heart failure; hence, these cells and their recruiting mechanisms are discussed as therapeutic targets. Leukocyte recruitment has been studied closely in the infarct; however; less is known about acute inflammation in the remote, nonischemic myocardium. Given that side-to-side slippage of myocytes,

See page 164

From the *Center for Systems Biology, Massachusetts General Hospital and Harvard Medical School, Boston, Massachusetts; †Department of Nuclear Medicine, Seoul National University Bundang Hospital, Seoul National University College of Medicine, Seoul, Korea; ‡Department of Cardiology, Academic Medical Center, University of Amsterdam, Amsterdam, the Netherlands; §Department of Pathology and Cardiac Surgery, ICaR-VU, VU University Medical Center, Amsterdam, the Netherlands; ‖Cardiac MR PET CT Program, Division of Cardiology and Department of Radiology, Massachusetts General Hospital, Boston, Massachusetts; and the ¶Division of Nuclear Medicine and Molecular Imaging, Department of Radiology, Brigham and Women's Hospital, Boston, Massachusetts. This work was funded in parts by grants from the National Institutes of Health (R01HL095629 and R01HL096576 to Dr. Nahrendorf, Translational Program of Excellence in Nanotechnology HHSN268201000044C, RO1EB006432, R24-CA92782 to Dr. Weissleder), AHA Scientist Development Grant to Dr. Nahrendorf, Korea Research Foundation Grant (KRF-2009-013-E00027) to Dr. Lee, and Deutsche Herzstiftung e.V. to Dr. Leuschner. All other authors have reported that they have no relationships relevant to the contents of this paper to disclose. The first two authors contributed equally to this work.

Manuscript received July 5, 2011; revised manuscript received August 17, 2011, accepted August 23, 2011.

JACC Vol. 59, No. 2, 2012
January 10, 2012:153–63

Abbreviations and Acronyms

^{18}FDG = 18-fluorodeoxyglucose
CT = computed tomography
FDG = fluorodeoxyglucose
MI = myocardial infarction
MRI = magnetic resonance imaging
PET = positron emission tomography

myocyte hypertrophy, myocyte apoptosis, and remodeling of the collagen matrix occur here and substantially contribute to the dilation of the heart after MI (3–6), the nonischemic myocardium deserves closer scrutiny. One reason for the limited insight into inflammatory processes after MI, at least in patients, is the paucity of imaging tools to study tissue levels of inflammatory cells (7).

Emerging hybrid positron emission tomography (PET)/magnetic resonance imaging (MRI) has considerable potential for cardiovascular imaging because it combines PET, a highly sensitive and quantitative modality that can follow rare molecular events (8,9), with MRI, which noninvasively assesses cardiovascular anatomy and function, infarct size, perfusion, myocardial strain, and metabolism with excellent spatial and temporal resolution (10–14). Combining both modalities could enhance preclinical research by providing multidimensional "systems" data and is also likely to directly impact clinical imaging (15–17). Here we devised a fusion method that relies on a fiducial vest developed for cardiovascular imaging in mice with separate scanners. We hypothesized that when glucose usage is suppressed in myocytes, the temporal and spatial 18-fluorodeoxyglucose (^{18}FDG) signal pattern may reflect inflammatory cell activity in the heart. We then explored the recruitment of monocytes to nonischemic remote myocardium after coronary ligation in mice, using imaging in conjunction with flow cytometric cell quantitation.

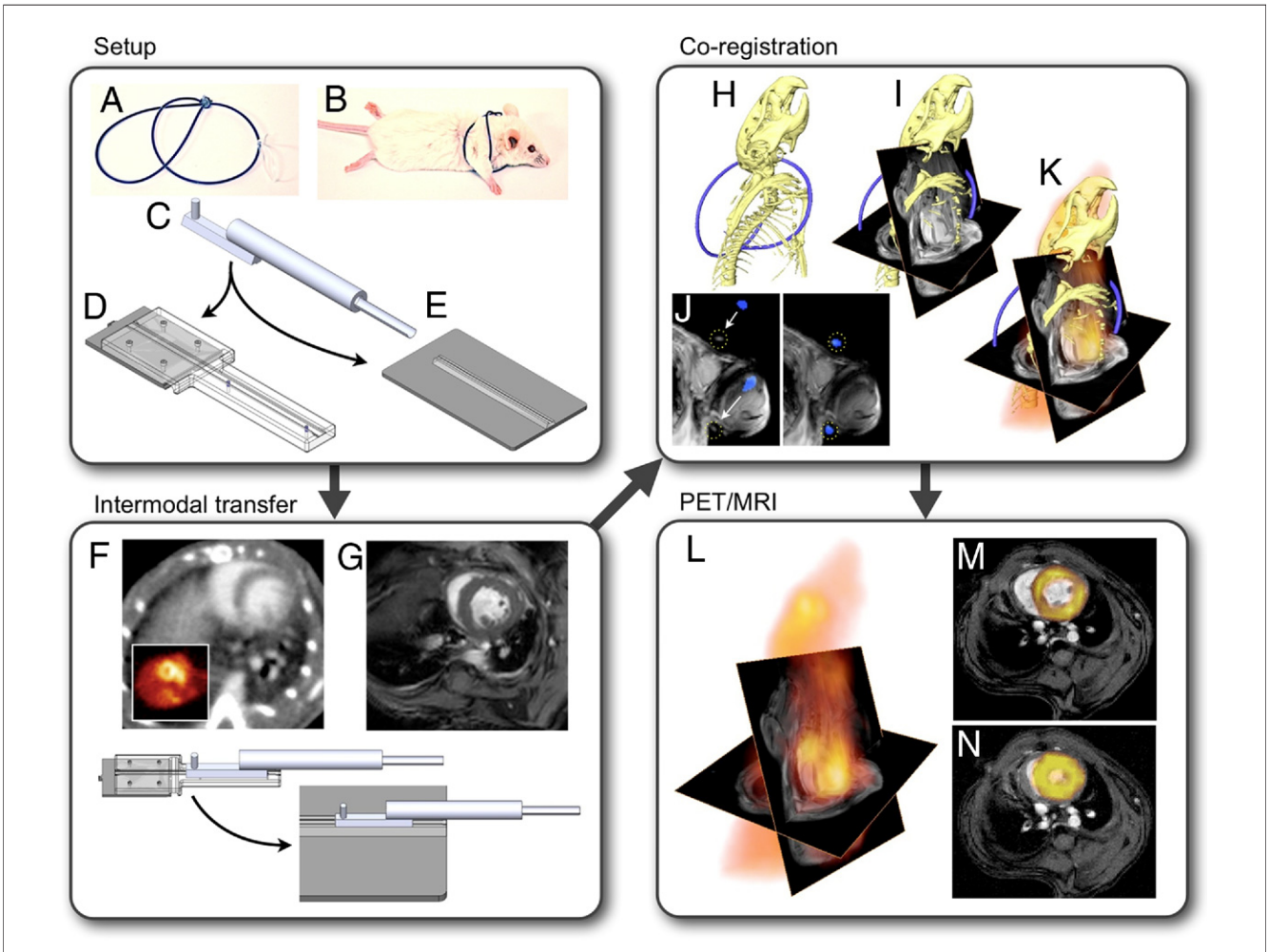

Figure 1 Experimental Set-Up

(A and B) Fiducial vest. **(C)** Multimodality imaging bed connects to gurneys on positron emission tomography/computed tomography (PET/CT) **(D)** and magnetic resonance imaging (MRI) **(E)** to allow for a no-touch transfer of the mouse between modalities **(F and G)**, ensuring that no major position changes hamper data fusion. **(H)** Three-dimensional CT data show the skeleton and a part of the fiducial marker in blue. **(I)** CT and MRI matrices are matched, and the angles used during cardiac MRI acquisition are applied. **(J)** Fiducials visible on CT and MRI are aligned. **(K)** Three-dimensional data from PET/CT/MRI. **(L)** CT information is phased out to yield PET/MRI. **(M and N)** Double-angulated diastolic and systolic PET/MRI short-axis views.

Methods

Please see the Online Appendix for additional information.

PET/computed tomography. Mice were imaged by microPET/computed tomography (CT) using an Inveon (Siemens Medical Solutions, Inc., Malvern, Pennsylvania) small-animal scanner 1 h after intravenous (IV) injection of 20.7 ± 0.9 MBq ^{18}FDG through the tail vein. CT preceded PET, acquiring 360 cone beam projections with a source power and current of 80 keV and 500 μA, respectively. Projections were reconstructed into 3-dimensional volumes containing 512 × 512 × 768 voxels with the dimension of 0.11 × 0.11 × 0.11 mm. Gated PET was acquired for 30 min using electrocardiogram leads and a respiratory pillow (m2m Imaging Corp., Cleveland, Ohio). A high-resolution Fourier rebinning algorithm was used to rebin sinograms, followed by a filtered back-projection algorithm for reconstruction. Image voxel size was 0.797 × 0.861 × 0.861 mm. Data were calculated as mean standardized uptake values.

Magnetic resonance imaging. We obtained delayed-enhancement cine images on a 7-T Bruker Pharmascan with electrocardiogram and respiratory gating (SA Instruments, Inc., Stony Brook, New York), a gradient echo FLASH sequence with the following imaging parameters: echo time 2.7 ms; 16 frames per R-R interval (repetition time 7.0 to 15 ms); resolution 200 μm × 200 μm × 1 mm; number of excitations 4; flip angle 60°. Imaging was done 10 to 20 min after IV injection of 0.3 mmol/kg gadolinium–diethylene triamine pentaacetic acid (Gd-DTPA) (19,20).

Registration/fusion. PET/MRI fusion was facilitated by a custom-designed mouse bed and a PET/CT gantry adapter. These hardware components facilitated intermodal transfer, minimized animal motion, and allowed us to center the mouse at nearly identical coordinates in MRI and PET/CT scanners. A "framed fusion" approach was then implemented (21) using external fiducial landmarks. The fiducials were provided by a custom-built "vest" (Fig. 1) made of several loops of PE50 tubing. The vest tightly surrounded the mouse's chest, providing a rigid frame that followed movements of the animal during transfer. The tubes were filled with 15% iodine in water, rendering them visible in both CT and MRI. The tubes' orientation was optimized to provide unique landmarks for MRI and CT data registration (outlined in Fig. 1). PET data were fused to CT as part of a standard PET/CT workflow. Registration of MRI and CT data sets was obtained by computing the rigid transformation necessary to superimpose the fiducials via a 2-step process. The first step accomplished rough alignment of data sets based on the holder position within each modality, followed by translational and rotational alignment via a cross-correlation algorithm. Fused data sets were used to place volumes of interest for quantitation of PET signal. Colocalization achieved by this procedure was tested with an ^{18}F phantom using the cross-correlation function (22). The peak correlation coefficient of 5 MRI and PET slices was 0.91 ± 0.02, implying excellent coregistration of signal distribution between PET and MRI (Fig. 2).

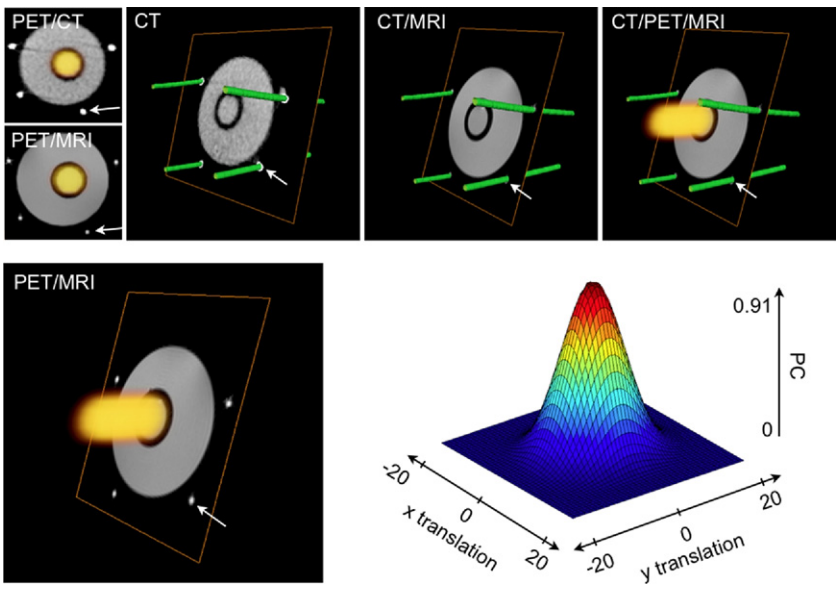

Figure 2 Colocalization

A 3-modality phantom was used to assess the developed work flow. Fiducials line the exterior of the phantom, which is composed of 2 concentric chambers. The outer chamber contains water only, and the inside contains ^{18}F. The mesh diagram displays the correlation of PET and MR signal after fusion. The data sets correlate with a Pearson correlation coefficient (PC) of 0.91 ± 0.02. When PET and MRI are translated along the y- or x-axis, the correlation drops rapidly. **Arrows** point at fiducial markers. Other abbreviations as in Figure 1.

Clinical PET/CT. Clinical PET/CT was obtained on day 5 after MI after obtaining informed consent and approval of the institutional committee. To limit myocyte uptake of ^{18}FDG, patients received a high-fat, low-carbohydrate diet the evening before imaging, fasted for 12 h before imaging, and were given beta-blockers IV and a lipid-rich drink (very low carbohydrate Atkins shake) 90 min before ^{18}FDG injection (23).

Flow cytometry. Flow cytometry was performed on days 1 to 14 post-MI (n = 3 to 4 per group) (24). Hearts were divided into MI and remote myocardium, digested in enzyme mixture, and passed through a cell strainer. Single-cell suspensions were stained with the following antibodies: CD11b-APC-Cy7, B220-PE, CD49b-PE, NK1.1-PE, CD90-PE, Ly-6G-PE, Ter119-PE, F4/80-PE-Cy7, and Ly-6C-FITC (BD Biosciences, San Jose, California). Monocytes/macrophages were defined as CD11b^{high} (B220/CD49b/NK1.1/CD90/Ly-6G/Ter119)^{low}. Monocyte subsets were identified as CD11b^{high} (B220/CD49b/NK1.1/CD90/Ly-6G/Ter119)^{low}F4/80^{low} Ly-6C^{high} or Ly-6C^{low}. Flow cytometry was performed using a multicolor flow cytometer (LSR II, BD Biosciences).

Measurement of activity in monocytes/macrophages isolated from infarcts. ^{18}FDG was injected IV (n = 6). Three hours later hearts were removed, and activity in infarcts was measured by gamma counting. Afterward, tissue was treated as described previously to produce cell suspensions. Cells were stained with CD11b-PE, followed by incubation with anti-PE magnetic beads (Miltenyi Biotec Inc., Auburn, California) and separated with MACS columns. Activity of magnetically retrieved cells was measured by gamma counting.

Cx3cr1$^{gfp/+}$ mice (n = 3) were used to measure the diameter of splenic monocytes (25) to calculate monocyte weight. This was necessary to compare cell and tissue activity, both normalized to weight. In mice anesthetized with isoflurane, the spleen was imaged with intravital

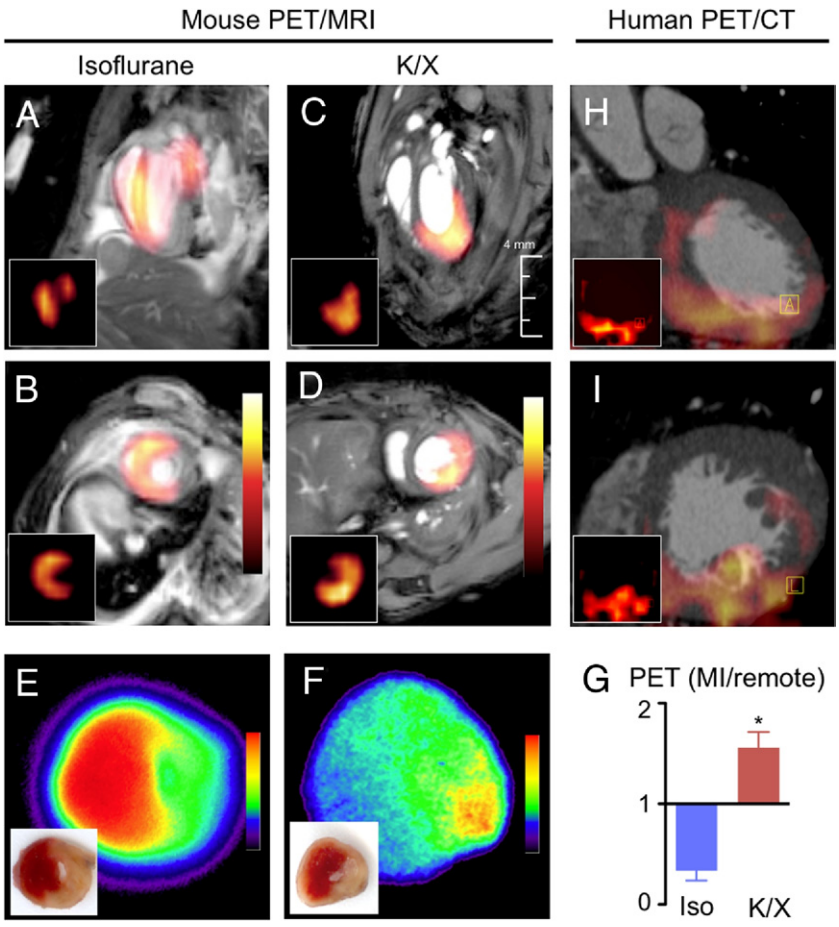

Figure 3 ^{18}FDG PET/Gd-DTPA MRI

(A to D) 18-fluorodeoxyglucose (^{18}FDG) PET/MRI long- and short-axis views acquired in mice on day 5 after myocardial infarction (MI) using different anesthesias. Insets show PET signal. MRI used delayed-enhancement cine gradient echo. Autoradiography of short-axis rings in mice with isoflurane (Iso) **(E)** vs. ketamine/xylazine (K/X) **(F)**. Insets depict the infarct as unstained pale tissue on triphenyltetrazolium chloride. **(G)** Infarct to remote myocardium standardized uptake value ratio in ^{18}FDG scans with respective anesthesia (mean ± SEM; *$p < 0.01$). **(H and I)** ^{18}FDG PET/CT in a patient 5 days after right coronary artery occlusion showed increased PET signal in the injured inferior left ventricular wall. Abbreviations as in Figure 1.

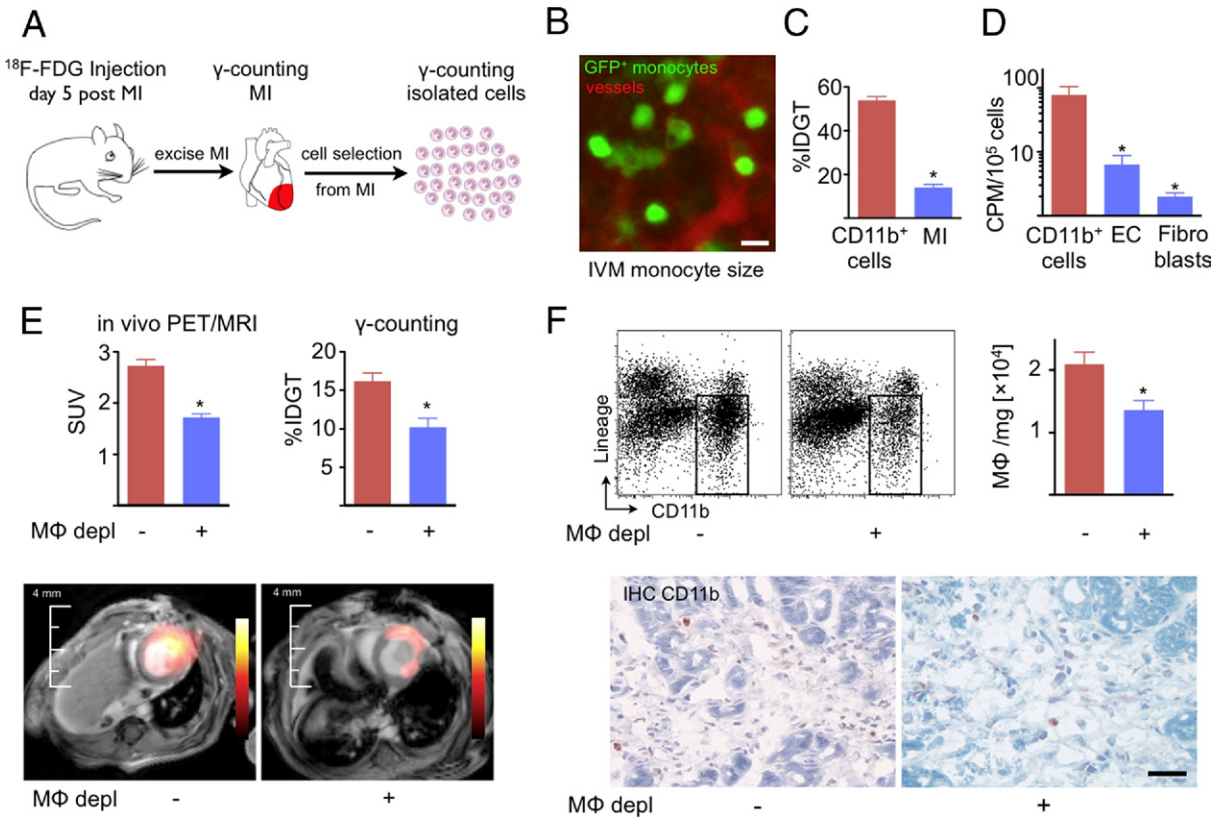

Figure 4 **^{18}FDG Uptake is Linked to Presence of CD11b^{+} Monocytes/Macrophages**

(A) Experimental set-up. Mice were injected, and activity in infarct was assessed by scintillation counting. Thereafter, CD11b^{+} monocytes/macrophages (MΦ) were isolated from the same infarct tissue by positive selection with antibodies coupled to magnetic beads. **(B)** To express gamma counts normalized to cellular weight, mean cell diameter was measured by intravital microscopy (IVM). The mean monocytic diameter was then used to calculate cell volume and weight. Scale bar = 15 μm. **(C)** Activity of monocytes/macrophages and the tissue from which they were isolated. **(D)** Counts per min (CPM) for cell types isolated from infarct tissue. **(E)** PET/MRI on day 5 after MI, followed by ex vivo counting. **(F)** Fluorescence-activated cell sorting enumeration **(upper panels)** and immunohistochemical (IHC) staining **(lower panels)** of monocytes/macrophages in infarcts (mean ± SEM; *p < 0.05). Scale bar = 30 μm. EC = endothelial cells; GFP = green fluorescent protein; %IDGT = percent injected dose/gram of tissue; MΦ depl = monocyte/macrophage depletion with clodronate liposomes; SUV = standardized uptake value; other abbreviations as in Figures 1 and 3.

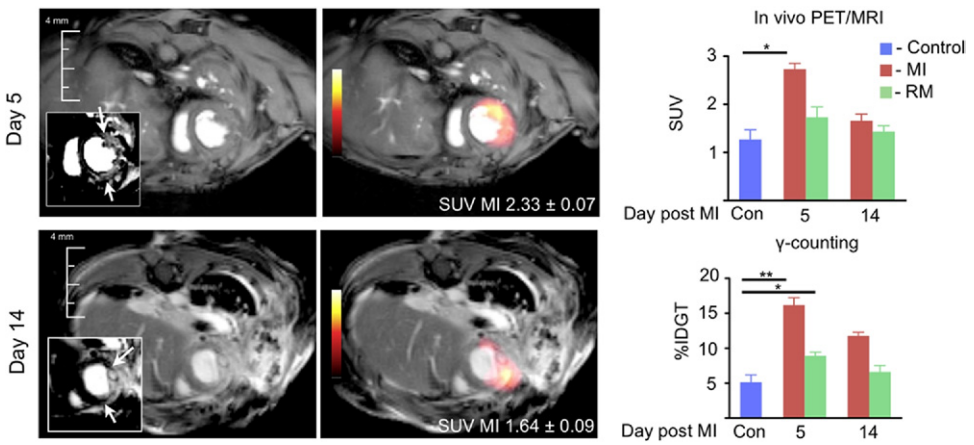

Figure 5 **^{18}FDG PET/MRI at Different Time Points After MI**

Arrows in insets point at infarct in delayed-enhancement MRI. Numbers in PET/MR images show the SUV of presented cases (mean ± SEM; *p < 0.05, **p < 0.01). Con = noninfarcted control group; %IDGT = % injected dose/gram tissue; RM = remote myocardium; other abbreviations as in Figures 1, 3, and 4.

JACC Vol. 59, No. 2, 2012
January 10, 2012:153–63

microscopy as previously described (26,27) using an intravital laser scanning microscope (IV100, Olympus).

Immunohistochemistry on human myocardial tissue. Myocardial tissue was collected from 11 patients with an infarct age of 5 to 14 days who were referred to the department of pathology, VU University Medical Center, Amsterdam, the Netherlands (mean age 62 ± 16 years, 45% male). Tissue was obtained from the infarct zone (left ventricle) and the remote myocardium (right ventricle). Of note, we cannot exclude that coronary arteries supplying the remote myocardium were completely free of disease in these patients. Control tissue was obtained from 8 patients who died from a cause not related to MI (4 men, mean age 61 ± 16 years, 50% male). None of the patients in this study received reperfusion therapy. The study was conducted in accordance with the Declaration of Helsinki, and the study protocol was approved by the institutional medical ethics committee. Tissue was fixed in formalin, embedded in paraffin, cut in 4-μm–thick sections, and stained with an antibody for human CD68 (Dako, Glostrup, Denmark). Quantification of macrophages was performed by counting the number of extravascular CD68$^+$ macrophages.

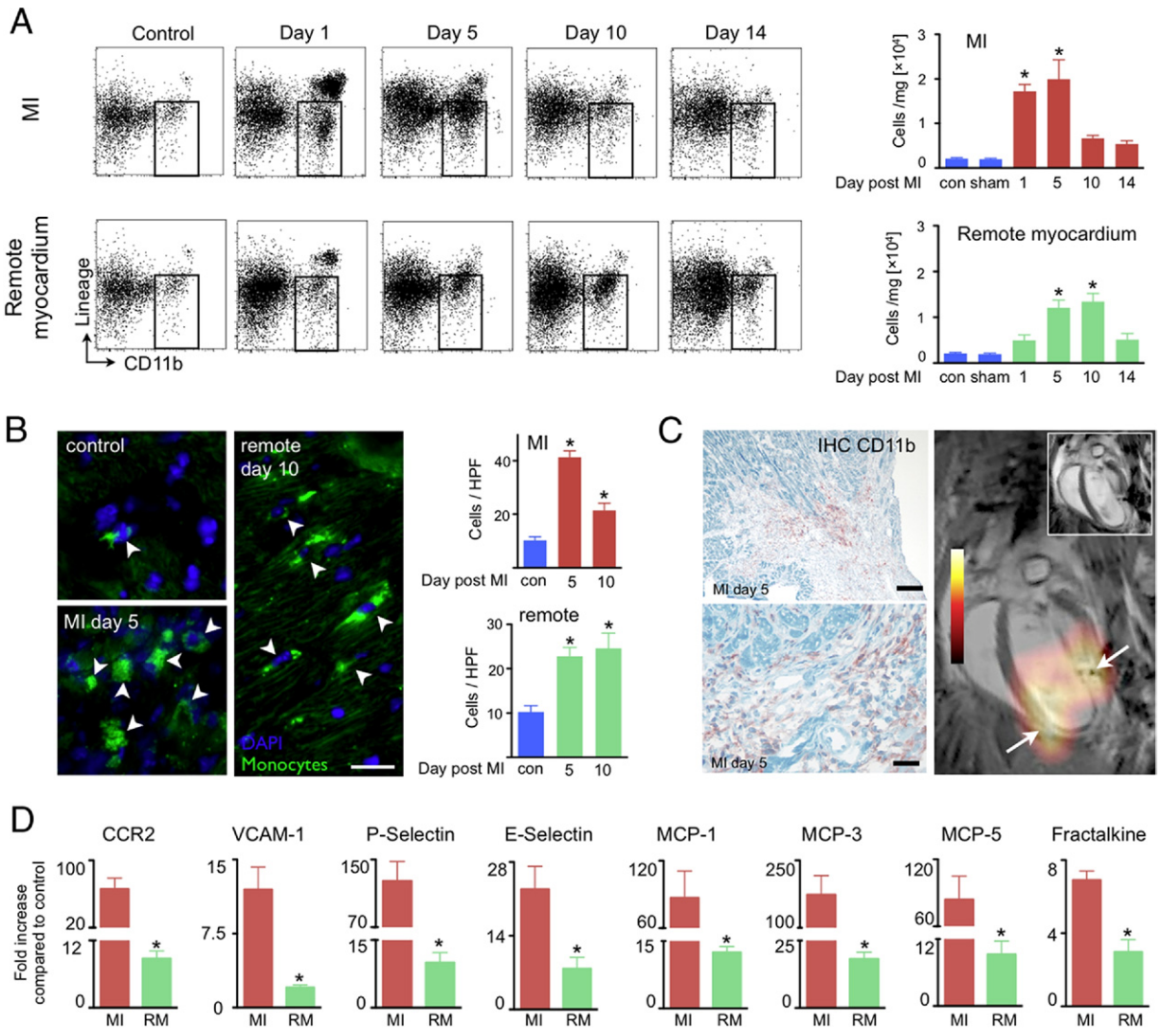

Figure 6 MΦ Accumulation in Infarct and Remote Myocardium

(A) Fluorescence-activated cell sorting analysis of CD11b$^+$ cells (gate in dot plots) at different time points in the infarct and remote myocardium. **(B)** Immunofluorescence microscopy of GFP$^+$ monocytes. Scale bar = 25 μm. Bar graphs show GFP$^+$ cells counted per high power field (HPF) at 200× magnification. **(C)** CD11b$^+$ cells are accentuated in the border zone, where we frequently observed high PET signals. Scale bar = 0.1 mm in **upper panel** and 30 μm in **lower panel**. On the right, delayed-enhancement MRI **(inset)** and PET/MRI long-axis view on day 5 with typical border zone **(arrows)** configuration of signal. **(D)** Quantitative reverse transcriptase polymerase chain reaction analysis in MI and nonischemic remote myocardium on day 5 after MI (mean ± SEM; *p < 0.05). CCR2 = chemokine (C-C motif) receptor 2; DAPI = 4',6-diamidino-2-phenylindole; MCP = monocyte chemoattractant protein; VCAM = vascular cellular adhesion molecule; other abbreviations as in Figures 1, 3, 4, and 5.

Results

Myocardial ^{18}FDG signal. PET/MR images (^{18}FDG PET combined with delayed-enhancement MRI after injection of Gd-DTPA) and ex vivo autoradiography in conjunction with triphenyltetrazolium chloride staining showed that ketamine/xylazine anesthesia suppressed uptake in the remote myocardium and unmasked the increased PET signal in infarcts on day 5 after MI (Fig. 3). Specifically, the infarct to remote myocardium signal ratio changed from 0.33 ± 0.1 with isoflurane to 1.56 ± 0.1 using ketamine/xylazine ($p < 0.05$) (Fig. 3G). To explore whether ^{18}FDG could be used to follow infarct inflammation in humans, we imaged a patient 5 days after inferior MI. In this patient, occlusive thrombosis of the right coronary artery was verified by x-ray coronary angiography and treated by placement of a stent. PET images showed increased ^{18}FDG signal within the inferior left ventricular wall (Figs. 3H and 3I).

^{18}FDG uptake in monocytes/macrophages. We performed several experiments to determine if monocytes/macrophages in the infarct contained ^{18}FDG after IV injection of the PET agent. First we isolated monocytes/macrophages from infarcts and measured activity in these purified cell populations as outlined in Figure 4A. Traditionally, reported tissue activity is normalized to weight. To calculate monocyte weight using the radius, volume, and density, we measured the diameter of monocytes by intravital microscopy (13.2 ± 1.0 μm) (Fig. 4B). The calculated average cellular weight was 1.3 ng. This number was then used to normalize ^{18}FDG activity to weight by multiplication with the cell number in the sample. The activity of cells isolated from infarcts was significantly higher than the activity of the infarct tissue from which they were retrieved (Fig. 4C). We also isolated monocyte/macrophages, endothelial cells, and fibroblasts from infarcts after IV ^{18}FDG injection. Scintillation counting revealed that the cellular activity was highest in monocytes/macrophages (Fig. 4D).

Next we depleted monocytes/macrophages with clodronate liposomes and imaged these mice on day 5 after MI. Depletion reduced the in vivo infarct activity by 34% (Fig. 4E). Scintillation counting of infarct tissue showed a 37% decrease of activity (Fig. 4E). Immunohistochemistry and flow cytometric enumeration confirmed a reduction of monocyte/macrophage numbers by 35%, comparable to the decrease in ^{18}FDG signal (Fig. 4F). On day 10 after MI, depletion reduced the infarct signal by 31% ($n = 6$ per group; $p < 0.05$).

Time course of ^{18}FDG PET signal. There was significantly increased uptake in the infarct of mice on day 5 after coronary ligation (standardized uptake value 2.7 ± 0.1) (Fig. 5) when compared with myocardium in control mice (1.3 ± 0.2; $p < 0.01$). On day 14, the ^{18}FDG signal approached control values (MI 1.6 ± 0.1; remote 1.4 ± 0.1). Scintillation counting corroborated the imaging results (Fig. 5). Interestingly, we found differences between the activity in noninfarcted remote myocardium on day 5 after MI and control hearts (percent injected dose/gram of tissue, remote 8.9 ± 0.5; control 5.1 ± 1.0; $p < 0.05$). The MRI component of hybrid datasets enabled the precise definition of the infarct area and analysis of anatomic and functional parameters. The infarct size was 30% ± 2% in the studied cohorts. Wall thickening was reduced in the infarcted area (remote 45% ± 5%; infarct 10% ± 5%; $p < 0.01$).

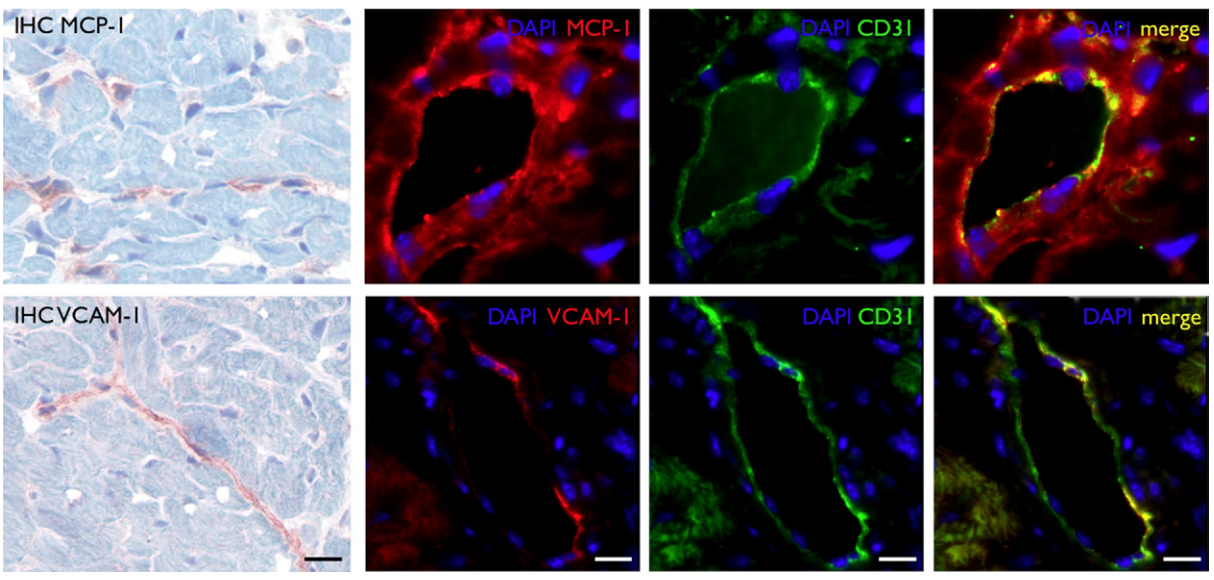

Figure 7 MCP-1 and VCAM-1 Expression in Remote Myocardium

On day 5 after MI, immunohistochemical and immunofluorescence staining showed expression of the chemokine and adhesion molecule, which colocalized with endothelial cells. Scale bar = 20 μm on IHC and 10 μm on immunofluorescence images. Abbreviations as in Figures 3, 4, 5, and 6.

JACC Vol. 59, No. 2, 2012
January 10, 2012:153–63

Monocyte/macrophage recruitment. Surprisingly, we found monocyte/macrophage recruitment in the noninfarcted remote myocardium (Fig. 6A). The number of $CD11b^+$ cells counted by fluorescence-activated cell sorting was lower than in the infarct and reached a later peak around day 10. Immunofluorescent cell quantitation by histology corroborated these findings (Fig. 6B). In some cases, monocyte/macrophages were most numerous in the border zone of the infarct (Fig. 6C), which may explain why we observed the peak PET signal at the edge of large infarcts (Fig. 6C).

Finding monocytes/macrophages in the nonischemic remote zone motivated us to study chemokine and adhesion molecule expression typically involved in cell recruitment (1). mRNA of chemokine (C-C motif) receptor 2 (CCR2), which is highly expressed by monocytes, was increased 66-fold in the infarct and 9-fold in the remote zone on day 5 after MI (Fig. 6D). P-Selectin, E-selectin and vascular cell adhesion molecule 1 (*VCAM-1*) expression were mildly increased (Fig. 6D). Monocyte chemoattractant protein 1 (*MCP-1*), *MCP-3*, *MCP-5*, and fractalkine were also upregulated in the remote zone when compared with control myocardium from noninfarcted hearts (12-fold, 18-fold, 9-fold, and 3-fold, respectively; $p < 0.05$) (Fig. 6D). Immunohistochemical and immunofluorescence studies showed expression of MCP-1 and VCAM-1 in the remote zone, which colocalized with endothelial cells (Fig. 7). Profiling for monocyte subsets in the remote myocardium revealed that Ly-$6C^{high}$ monocytes were recruited early and were followed by Ly-$6C^{low}$ monocytes, which peaked at day 10 after MI, approximately 5 days later when compared with cell dynamics in the infarct (Fig. 8). Analysis of clinical specimens obtained from autopsy cases after acute MI revealed robust recruitment of $CD68^+$ macrophages to the noninfarcted myocardium in patients (Fig. 9).

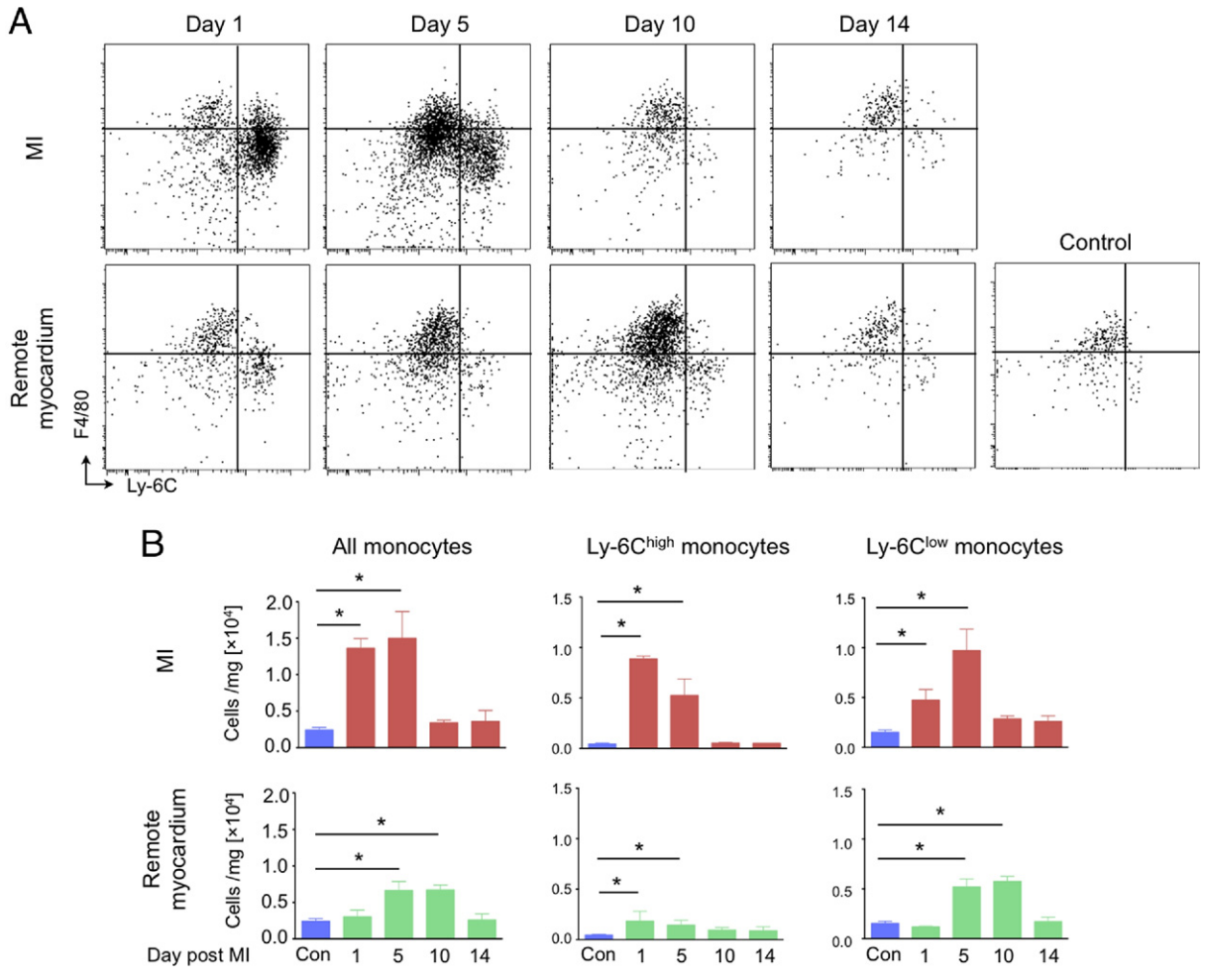

Figure 8 Monocyte Subsets in Remote Myocardium

(A) Fluorescence-activated cell sorting dot plots gated on $CD11b^+$ $lineage^-$ cells showed serial change of MΦ in MI and remote myocardium. Control = noninfarcted mouse. **(B)** Bar graphs of absolute number of monocyte subsets in MI and remote myocardium (mean ± SEM; *$p < 0.05$). Abbreviations as in Figures 3, 4, and 5.

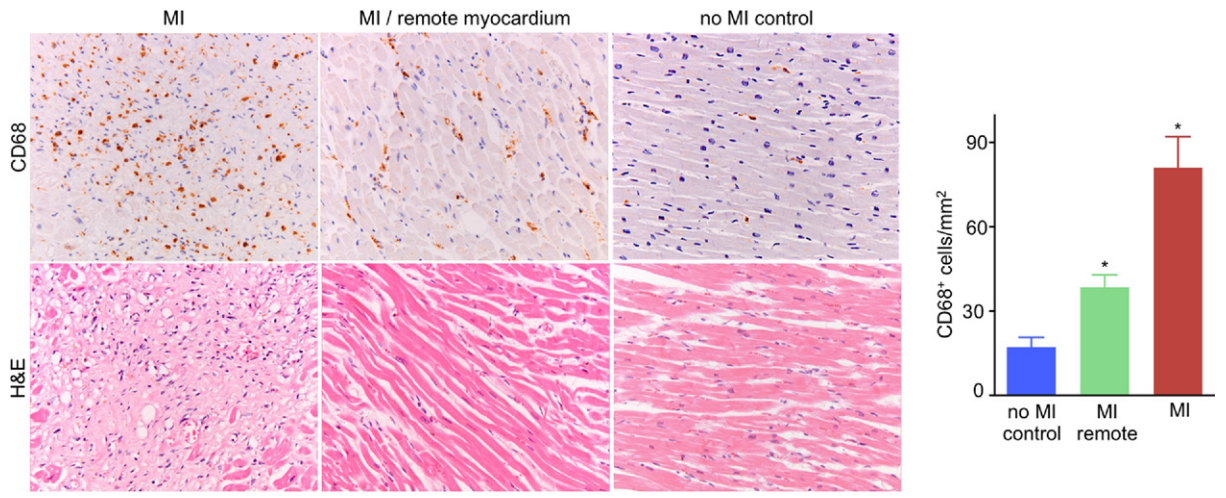

Figure 9 **CD68$^+$ Cells in Heart Tissue of Patients**

Histology images of immunoreactive CD68 staining **(top row)** and hematoxylin and eosin (H&E) staining **(bottom row)** at 200× magnification (mean ± SEM; *$p < 0.05$). The **graph** displays quantification of CD68$^+$ cells in respective cardiac tissue samples from patients with MI. Abbreviation as in Figure 3.

Protease activity. Finally, we assessed the activity of matrix metalloproteinase (MMP)-2 and MMP-9 using an activatable fluorescence reporter. Although fluorescence intensity was highest in the infarct, we found significant activation of the probe in the remote zone and septum (Fig. 10).

Discussion

The data presented here reflected the spatial and temporal kinetics of innate immune cells after MI and explored the use of ^{18}FDG PET for following infarct inflammation. Early after ischemia, monocytes and macrophages infiltrated injured tissue in large numbers. These innate immune cells are emerging as key regulators of infarct healing (1,2). Previous studies have shown that monocytes/macrophages are present in the ischemic myocardium during the first 2 weeks after ischemic injury and orchestrate tissue repair (18,24). They remove debris, enhance neoangiogenesis, release a myriad of inflammatory cytokines, and are a major source of proteases that regulate the turnover of extracellular matrix. Preclinical studies have revealed that proper infarct healing calls for a delicate balance of monocyte activity (2). Excessive as well as insufficient monocyte/macrophage numbers in the infarct compromise cardiac repair and lead to infarct expansion, aggressive left ventricular dilation, and ultimately, heart failure. Studies correlating the number of circulating blood pool monocytes at the time of infarction with clinical outcome have suggested that the preceding preclinical data reflect infarct healing in patients (28–30).

Although the presence, time course, and function of innate immune cells in the infarct have been well described, our finding of inflammation in the remote zone is new and somewhat surprising. The number of monocytes/

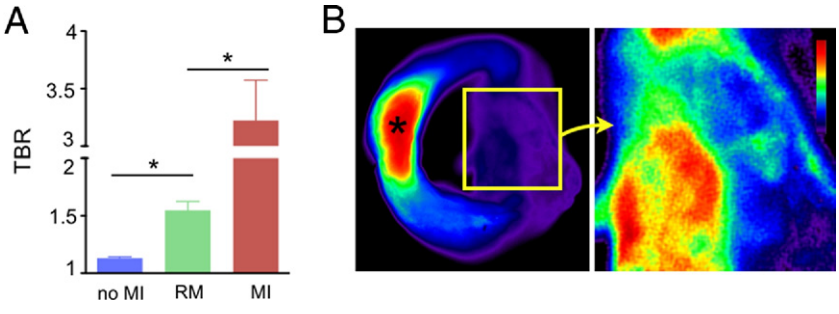

Figure 10 **Matrix Metalloproteinase Activity in Remote Myocardium**

(A) Target to background ratio (TBR) after injection of protease sensor (mean ± SEM; *$p < 0.05$). **(B)** Fluorescence reflectance image of short-axis ring 6 days after MI shows protease sensor activation in the remote myocardium **(inset, right panel)** (mean ± SEM; *$p < 0.05$). *MI. Abbreviations as in Figures 3 and 5.

macrophages in the noninfarcted myocardium was lower than in the ischemic tissue; however, their numbers detected by flow cytometry were substantial (approximately 10^4 per mg of tissue, 5.6-fold higher than in control mice). The time course was in accordance with the 2 monocytic phases described in the infarct (24), but the kinetics were slower. Peak cell numbers were reached on day 10 after MI, 5 days later than in the ischemic zone. Exploring the mechanism of recruitment, we also found increased expression of adhesion molecules and the chemokines known to recruit monocytes into the infarct (1,2). Tissue obtained from clinical autopsies showed a robust increase of macrophages in the remote myocardium of patients that died on day 5 to 14 after the ischemic event. The finding of higher MMP activity in the remote zone of mice indicated that these inflammatory processes are involved in remodeling of the left ventricle after ischemic injury, although the precise cellular contribution of MMP activity is unclear at this point. Future studies are required to dissect the molecular mechanism of how inflammation in the nonischemic myocardium is triggered. The expression of recruiting molecules such as VCAM-1 and MCP-1 argues against a mere "spill over" effect from the infarct. One could speculate that apoptosis of remote myocytes may trigger cell recruitment or that systemically increased angiotensin 2 activates endothelium in the remote zone.

We presented data showing that within subacutely infarcted myocardium, ^{18}FDG accumulated relative to the tissue's monocyte/macrophage content. PET signal changed synchronously with the number of innate immune cells, mirrored their typical spatial distribution after MI, and decreased in scale to cell numbers in a monocyte/macrophage depletion experiment. Furthermore, monocytes/macrophages isolated from infarcts showed high ^{18}FDG uptake. This evidence suggested that the infarct signal on day 5 after ischemia reflects—at least in part—inflammatory activity. Because ^{18}F decays with a half-life of 110 min, serial noninvasive spatiotemporal imaging of inflammation appears feasible.

The use of ^{18}FDG to image inflammation in myocardium has limitations. Myocytes can metabolize glucose and therefore show high ^{18}FDG uptake. Residual viable myocytes in the infarct may contribute to signal. Accordingly, suppression of this uptake is a prerequisite for imaging of inflammatory cells. Clinically, methods suppressing myocardial uptake have been developed to image inflammation in coronary arteries (23,31), and the clinical PET/CT case discussed in Figure 3 suggests that these strategies may also prove useful for imaging inflammation in the myocardium. Acutely ischemic and hibernating myocardium shifts its metabolic use of fatty acids toward glucose (32), which results in increased ^{18}FDG uptake and may change the observed relationship between ^{18}FDG uptake and monocyte/macrophage activity. Novel PET tracers that specifically target monocytes/macrophages could overcome these limitations (33,34); however, ^{18}FDG is clinically approved and could be explored now.

Conclusions

The obtained data showcased the synergy created by fusing high-resolution cardiac PET with MRI. Using separate systems and offline fusion circumvents engineering challenges faced in hybrid scanners, in which deploying PET in a magnetic field currently compromises sensitivity. Combining leading modalities for molecular and anatomic cardiovascular imaging holds promise for a number of interesting future applications. Data on cardiac metabolism, molecular pathways, cell populations, or drug targets could be integrated with parameters such as myocardial motion, strain, torsion, or perfusion. Such integration could foster modeling and systems biology approaches to provide novel insight into better treating heart failure.

Acknowledgments

The authors gratefully thank Paul Kennedy (PerkinElmer), Dustin Osbourne (Siemens), and Greg Wojtkiewicz (CSB).

Reprint requests and correspondence: Drs. Matthias Nahrendorf or Ralph Weissleder, Center for Systems Biology, 185 Cambridge Street, Boston, Massachusetts 02114. E-mail: mnahrendorf@mgh.harvard.edu or rweissleder@mgh.harvard.edu.

REFERENCES

1. Frangogiannis NG, Smith CW, Entman ML. The inflammatory response in myocardial infarction. Cardiovasc Res 2002;53:31–47.
2. Nahrendorf M, Pittet MJ, Swirski FK. Monocytes: protagonists of infarct inflammation and repair after myocardial infarction. Circulation 2010;121:2437–45.
3. Pfeffer MA, Braunwald E. Ventricular remodeling after myocardial infarction. Experimental observations and clinical implications. Circulation 1990;81:1161–72.
4. Jourdan-Lesaux C, Zhang J, Lindsey ML. Extracellular matrix roles during cardiac repair. Life Sci 2010;87:391–400.
5. Jugdutt BI. Ventricular remodeling after infarction and the extracellular collagen matrix: when is enough enough? Circulation 2003;108:1395–403.
6. Anversa P, Kajstura J, Olivetti G. Myocyte death in heart failure. Curr Opin Cardiol 1996;11:245–51.
7. Leuschner F, Nahrendorf M. Molecular imaging of coronary atherosclerosis and myocardial infarction: considerations for the bench and perspectives for the clinic. Circ Res 2011;108:593–606.
8. Sanz J, Fayad ZA. Imaging of atherosclerotic cardiovascular disease. Nature 2008;451:953–7.
9. Nahrendorf M, Sosnovik DE, French BA, et al. Multimodality cardiovascular molecular imaging, part II. Circ Cardiovasc Imaging 2009;2:56–70.
10. Bandettini WP, Arai AE. Advances in clinical applications of cardiovascular magnetic resonance imaging. Heart 2008;94:1485–95.
11. Hays AG, Hirsch GA, Kelle S, Gerstenblith G, Weiss RG, Stuber M. Noninvasive visualization of coronary artery endothelial function in healthy subjects and in patients with coronary artery disease. J Am Coll Cardiol 2010;56:1657–65.
12. Kim HW, Farzaneh-Far A, Kim RJ. Cardiovascular magnetic resonance in patients with myocardial infarction: current and emerging applications. J Am Coll Cardiol 2009;55:1–16.
13. Rehwald WG, Wagner A, Sievers B, Kim RJ, Judd RM. Cardiovascular MRI: its current and future use in clinical practice. Expert Rev Cardiovasc Ther 2007;5:307–21.

14. Stuber M, Weiss RG. Coronary magnetic resonance angiography. J Magn Reson Imaging 2007;26:219–34.
15. Catana C, Procissi D, Wu Y, et al. Simultaneous in vivo positron emission tomography and magnetic resonance imaging. Proc Natl Acad Sci U S A 2008;105:3705–10.
16. Judenhofer MS, Wehrl HF, Newport DF, et al. Simultaneous PET-MRI: a new approach for functional and morphological imaging. Nat Med 2008;14:459–65.
17. Buscher K, Judenhofer MS, Kuhlmann MT, et al. Isochronous assessment of cardiac metabolism and function in mice using hybrid PET/MRI. J Nucl Med 2010;51:1277–84.
18. Panizzi P, Swirski FK, Figueiredo JL, et al. Impaired infarct healing in atherosclerotic mice with Ly-6C(hi) monocytosis. J Am Coll Cardiol 2010;55:1629–38.
19. Yang Z, Berr SS, Gilson WD, Toufektsian MC, French BA. Simultaneous evaluation of infarct size and cardiac function in intact mice by contrast-enhanced cardiac magnetic resonance imaging reveals contractile dysfunction in noninfarcted regions early after myocardial infarction. Circulation 2004;109:1161–7.
20. Nahrendorf M, Sosnovik D, Chen JW, et al. Activatable magnetic resonance imaging agent reports myeloperoxidase activity in healing infarcts and noninvasively detects the antiinflammatory effects of atorvastatin on ischemia-reperfusion injury. Circulation 2008;117:1153–60.
21. Kessler ML, Pitluck S, Petti P, Castro JR. Integration of multimodality imaging data for radiotherapy treatment planning. Int J Radiat Oncol Biol Phys 1991;21:1653–67.
22. Nahrendorf M, Keliher E, Marinelli B, et al. Hybrid PET-optical imaging using targeted probes. Proc Natl Acad Sci U S A 2010;107:7910–5.
23. Rogers IS, Nasir K, Figueroa AL, et al. Feasibility of FDG imaging of the coronary arteries: comparison between acute coronary syndrome and stable angina. J Am Coll Cardiol Img 2010;3:388–97.
24. Nahrendorf M, Swirski FK, Aikawa E, et al. The healing myocardium sequentially mobilizes two monocyte subsets with divergent and complementary functions. J Exp Med 2007;204:3037–47.
25. Luster AD, Alon R, von Andrian UH. Immune cell migration in inflammation: present and future therapeutic targets. Nat Immunol 2005;6:1182–90.
26. Swirski FK, Nahrendorf M, Etzrodt M, et al. Identification of splenic reservoir monocytes and their deployment to inflammatory sites. Science 2009;325:612–6.
27. Leuschner F, Panizzi P, Chico-Calero I, et al. Angiotensin-converting enzyme inhibition prevents the release of monocytes from their splenic reservoir in mice with myocardial infarction. Circ Res 2010;107:1364–73.
28. Maekawa Y, Anzai T, Yoshikawa T, et al. Prognostic significance of peripheral monocytosis after reperfused acute myocardial infarction: a possible role for left ventricular remodeling. J Am Coll Cardiol 2002;39:241–6.
29. Mariani M, Fetiveau R, Rossetti E, et al. Significance of total and differential leucocyte count in patients with acute myocardial infarction treated with primary coronary angioplasty. Eur Heart J 2006;27:2511–5.
30. Tsujioka H, Imanishi T, Ikejima H, et al. Impact of heterogeneity of human peripheral blood monocyte subsets on myocardial salvage in patients with primary acute myocardial infarction. J Am Coll Cardiol 2009;54:130–8.
31. Wykrzykowska J, Lehman S, Williams G, et al. Imaging of inflamed and vulnerable plaque in coronary arteries with ^{18}F-FDG PET/CT in patients with suppression of myocardial uptake using a low-carbohydrate, high-fat preparation. J Nucl Med 2009;50:563–8.
32. Peterson LR, Gropler RJ. Radionuclide imaging of myocardial metabolism. Circ Cardiovasc Imaging 2010;3:211–22.
33. Nahrendorf M, Keliher E, Marinelli B, et al. Detection of macrophages in aortic aneurysms by nanoparticle positron emission tomography-computed tomography. Arterioscler Thromb Vasc Biol 2011;31:750–7.
34. Nahrendorf M, Zhang H, Hembrador S, et al. Nanoparticle PET-CT imaging of macrophages in inflammatory atherosclerosis. Circulation 2008;117:379–87.

Key Words: inflammation ■ myocardial infarction ■ PET/MRI ■ remote myocardium.

APPENDIX

For supplementary methods information, please see the online version of this article.